Applied Catalysis B: Environmental 123–124 (2012) 214–220

Contents lists available at SciVerse ScienceDirect

Applied Catalysis B: Environmental

journal homepage: www.elsevier.com/locate/apcatb

Synthesis and characterization of carbon riveted Pt/MWCNTs@TiO_2–TiC catalyst with high durability for PEMFCs application

Zheng-Zhi Jiang[a,b], Zhen-Bo Wang[a,*], Wei-Li Qu[a,b], Da-Ming Gu[b], Ge-Ping Yin[a]

[a] School of Chemical Engineering and Technology, Harbin Institute of Technology, No. 92 West-Da Zhi Street, Harbin 150001, China
[b] School of Science, Harbin Institute of Technology, No. 92 West-Da Zhi Street, Harbin 150001, China

ARTICLE INFO

Article history:
Received 2 December 2011
Received in revised form 19 March 2012
Accepted 24 April 2012
Available online 1 May 2012

Keywords:
Electrocatalysts
TiC
Multi-walled carbon nanotubes
Proton exchange membrane fuel cells

ABSTRACT

Pt/TiC, Pt/TiO_2–TiC, and Pt/MWCNTs@TiO_2–TiC catalysts have been synthesized by the microwave-assisted polyol process. Moreover, carbon riveted Pt/MWCNTs@TiO_2–TiC catalyst based on in situ carbonization of glucose has also been prepared. X-ray diffraction, energy dispersive analysis of X-ray, transmission electron microscopy, X-ray photoelectron spectroscopy, cyclic voltammograms, and accelerated potential cycling tests have been used to characterize the catalysts. Experimental results show that both of the activity and stability of Pt/TiC catalyst cannot meet the requirements of proton exchange membrane fuel cells. In comparison with Pt/TiC, Pt/TiO_2–TiC catalyst exhibits lower activity due to poor conductivity of TiO_2 and higher stability ascribed to strong metal–support interaction (SMSI) between Pt and TiO_2. However, compared with Pt/TiC, Pt/MWCNTs@TiO_2–TiC catalyst exhibits both higher activity and stability because of high electrical conductivity of the mixed support and SMSI between Pt nanoparticles and nanocapsule composite MWCNTs@TiO_2. Furthermore, the measurement results show that carbon riveted Pt/MWCNTs@TiO_2–TiC catalyst with similar activity to the Pt/C and Pt/TiO_2–C ones possesses 8.5 times stability as high as that of Pt/C and exhibits 4.5 times life-span as long as that of carbon riveted Pt/TiO_2–C reported in our previous study.

1. Introduction

Growing concerns over energy crisis and exposure to environmental pollution have drawn much attention to the development of proton exchange membrane fuel cells (PEMFCs) which have many advantages such as high energy density, low-temperature operation, fast start-up, simple structure, and convenient manipulation over other power sources [1–7]. There are two major obstacles including high cost and short life that hinder the world-wide commercialization of PEMFCs [8–11].

Supported catalysts which can improve the utilization of noble metal Pt and then reduce the total cost have been developed and applied to PEMFCs [10,12–16]. To date, the most widely used supports for Pt based catalysts are still carbon materials which are prone to be oxidized in the rigorous working environment of PEMFCs [17–19]. To mitigate corrosion of the catalyst supports and improve durability of the catalysts, more stable and corrosion-resistant supports such as titanium diboride [10], titanium nitride [20], tungstic oxide [21], vanadium oxide [22], indium tin oxide [23] and some composite ones [24,25] have attracted increasing interest.

Titanium carbide (TiC) has been widely used in the field of material modification due to the advantages of high hardness, high melting point, low density, and high chemical stability [26,27]. Moreover, TiC has been employed as the catalyst support for an iridium (Ir) electrocatalyst in a proton exchange membrane water electrolyser (PEMWE) [28]. The experimental results indicate that TiC is a chemically and electrochemically inert material in the whole range of experimental potentials between −0.4 V and 1.5 V [28]. Nevertheless, there are still very few publications on the field of TiC as the catalyst support for PEMFCs. It is very worth investigating about effect of TiC on the performance of Pt/TiC catalyst.

Herein, Pt/TiC catalyst for PEMFCs has been synthesized by the microwave-assisted polyol process (MAPP). The results of cyclic voltammograms (CV) and accelerated potential cycling tests (APCT) indicate that the activity of Pt/TiC catalyst is lower than Pt/C prepared by the same procedure due to the ordinary electrical conductivity of TiC and its stability is higher than Pt/C ascribed to the electrochemical stability of TiC. However, the performance of Pt/TiC cannot meet the requirements of commercialization of PEMFCs put forward by Department of Energy (DoE) of USA that the life-span of PEMFCs for transportation and for stationary application should be more than 5000 h and 40,000 h, respectively [29]. To enhance

* Corresponding author. Tel.: +86 451 86417853; fax: +86 451 86418616.
E-mail address: wangzhenbo1008@yahoo.com.cn (Z.-B. Wang).

0926-3373/$ – see front matter © 2012 Elsevier B.V. All rights reserved.
http://dx.doi.org/10.1016/j.apcatb.2012.04.040

the performance of Pt/TiC, TiC were mixed with multi-walled carbon nanotubes (MWCNTs) with remarkable electrical conductivity and TiO_2 which possesses strong metal–support interaction (SMSI) with Pt for preparing Pt/MWCNTs@TiO_2–TiC catalyst with both high activity and stability in this paper.

In our recent studies [30–32], a method on the basis of in situ carbonization of glucose to strengthen the support region of the catalyst without blocking of active catalytic sites has been reported. As-prepared Pt/MWCNTs@TiO_2–TiC catalyst was also subjected to the treatment of in situ carbonization of glucose. Carbon riveted Pt/MWCNTs@TiO_2–TiC catalyst has been characterized by X-ray diffraction, energy dispersive analysis of X-ray diffraction, transmission electron microscopy, X-ray photoelectron spectroscopy, cyclic voltammograms, and accelerated potential cycling tests.

2. Experimental

2.1. Materials preparation

2.1.1. Synthesis of Pt/TiC, Pt/TiO_2–TiC and Pt/MWCNTs@TiO_2–TiC

Hexachloroplatinic acid ($H_2PtCl_6{\cdot}6H_2O$) was purchased from Shanghai, China. TiC with particle size of 50 nm and TiO_2 with particle size of 20 nm were obtained from Xuan Cheng Jing Rui New materials Co., Ltd., China. Multi-walled carbon nanotubes (with outer diameter size of more than 50 nm and inner diameter size of about 30 nm) was obtained from Chengdu, China and 5 wt.% Nafion solution was purchased from Dupont. Except where specified, all chemicals were of analytical grade and used as received. Pt/TiC catalyst with the Pt metal loading of 20 wt.% was synthesized by the microwave-assisted polyol process [29–32]. Synthetic procedure in detail is shown as follows: 80 mg TiC was dispersed into the mixture of ethylene glycol (EG) and isopropyl alcohol under ultrasonic treatment (from Shanghai, 53 kHz, 280 W) for 1 h. Then H_2PtCl_6-EG solution (0.038 mol L^{-1}) was added into the uniform ink with urgent agitation for 3 h. The pH value (pHS-32 meter) of the ink was then adjusted to 12.0 by 1 mol L^{-1} NaOH-EG solution drop by drop and the suspension was subjected to consecutive microwave heating (from Galanz Ltd., 800 W) for 50 s. After cooling to room temperature, the pH value of the solution was adjusted to 3–4 by 0.1 mol L^{-1} HNO_3. The mixture was kept stirring for 12 h and then the product was washed repeatedly with ultrapure water (Millipore, 18.2 MΩ cm). The 20 wt.% Pt/TiO_2–TiC and Pt/MWCNTs@TiO_2–TiC catalysts were synthesized by the same process for preparing Pt/TiC, but TiC was replaced by the mixture of TiO_2 and TiC or the mixture of MWCNTs, TiO_2, and TiC, respectively. After the mixture of MWCNTs, TiO_2, and TiC was ultrasonicated for 2 h and agitated for 2 h, TiO_2 entered the inside of MWCNTs because the inner diameter of MWCNTs is larger than the particle size of TiO_2 [32]. After TiO_2 entered the inside of MWCNTs, the nanocapsule composite of MWCNTs@TiO_2 was formed due to the interaction between MWCNTs and TiO_2 [32] and then the mixed support became the mixture of TiC and the nanocapsule composite of MWCNTs@TiO_2. The obtained Pt/TiC, Pt/TiO_2–TiC, and Pt/MWCNTs@TiO_2–TiC catalysts were dried for 3 h at 80 °C and then stored in a vacuum vessel.

2.1.2. Preparation of carbon riveted Pt/MWCNTs@TiO_2–TiC catalyst

The carbon riveted Pt/MWCNTs@TiO_2–TiC catalyst was synthesized in accordance with our recent reports [30,32]. The synthetic process is shown as follows: firstly, 50 mg Pt/MWCNTs@TiO_2–TiC catalyst and 8.3 mg glucose ($C_6H_{12}O_6{\cdot}H_2O$) were dispersed into 10 mL H_2O (Millipore, 18.2 MΩ cm) in 50 mL beaker under ultrasonic treatment for 1 h to form uniform slurry. The slurry was first dried at 70 °C in a porcelain boat and then heated at 400 °C for 1 h in the tube furnace under argon. After it was cooled to room temperature in argon, the catalyst was stored under vacuum.

2.2. Physical characterizations

2.2.1. X-ray diffraction (XRD)

The D/max-RB diffractometer (made in Japan) using a Cu K*a* X-ray source operating at 45 kV and 100 mA, scanning at a rate of 4° min^{-1} with an angular resolution of 0.05° was used to obtain the XRD patterns of all catalysts.

2.2.2. Energy dispersive analysis of X-ray (EDAX)

Scanning electron microscope (SEM, Hitachi Ltd. S-4700) was equipped with a hitachi-S-4700 analyzer for a rapid EDAX analysis of chemical composition. The samples were supported on the aluminium foil to eliminate the influence of the conductive carbon tape. The sample surface was impinged from the normal angle for 100 s by the X-ray incident electron beam with energies ranging from 3 to 30 keV.

2.2.3. Transmission electron microscopy (TEM)

TEM pictures of all catalysts were characterized using a TECNAI G2 F30 field emission transmission electron microscope operated at 300 kV. The samples for TEM analysis were prepared by ultrasonically dispersing the catalyst powder in ethanol. A drop of the suspension was deposited on a standard copper grid coated with carbon film. The copper grid was then dried overnight.

2.2.4. X-ray photoelectron spectroscopy (XPS)

To determine the surface properties of the catalysts, XPS analysis was carried out using the Physical Electronics PHI model 5700 instrument. Before XPS analysis, all samples were dried under vacuum at 80 °C overnight. The take-off angle of the sample to analyzer was 45° and the Al X-ray source was operated at 250 W. Survey spectra were collected at a pass energy (PE) of 187.85 eV over a binding energy range from 0 eV to 1300 eV. High binding energy resolution multiplex data for the individual elements were collected at a PE of 29.55 eV. During all XPS experiments, the pressure inside the vacuum system was maintained at 1×10^{-9} Pa.

2.3. Electrochemical measurements

In a conventional three-electrode cell, electrochemical measurements of all catalysts were performed with a CHI 650D instrument. Porous electrodes were prepared as follows: 5.0 mg catalyst in 2.5 mL ethanol was ultrasonicated for 20 min to form uniform ink. 10 μL of this ink was transferred onto a glassy carbon disk (GC, 4 mm diameter) and then 5 μL of the dilute aqueous Nafion® solution (5 wt.% solution in a mixture of lower aliphatic alcohols and ultrapure water) was added onto the GC. A piece of Pt foil (1 cm^2) was used as the counter electrode and the Hg/Hg_2SO_4 (−0.68 V relative to reversible hydrogen electrode, RHE) was applied as the reference electrode. The cyclic voltammograms within a potential range from −0.66 V to 0.49 V were recorded to calculate the electrochemical active specific surface area (ESA) [31,32]. The accelerated potential cycling tests which was conducted within the potential range of −0.11–0.49 V was applied to evaluate the stability of a catalyst. All experiments were carried out at a temperature of 25 ± 1 °C and all the potentials reported here were relative to the Hg/Hg_2SO_4 electrode.

3. Results and discussion

Schematic diagram of carbon riveting process (CRP) and the detailed experimental procedure were shown in our recent studies [30,32]. For the sake of convenience and concision,

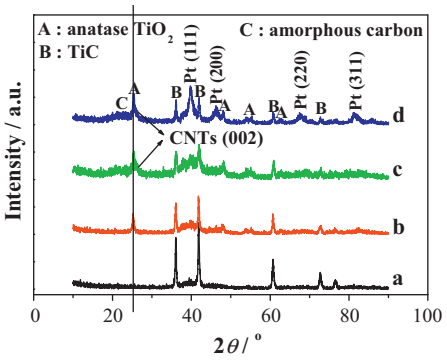

Fig. 1. XRD patterns of S1 (a), S2 (b), S3 (c), and S4 (d) catalysts.

Pt/TiC, Pt/TiO_2–TiC, Pt/MWCNTs@TiO_2–TiC, and carbon riveted Pt/MWCNTs@TiO_2–TiC catalysts are designated as S1, S2, S3, and S4, respectively. Representative diffraction peaks of Pt [(1 1 1), (2 0 0), (2 2 0), and (3 1 1)] are distinctly observed in all XRD patterns as shown in Fig. 1, meaning that Pt forms the face-centered cubic (fcc) crystal structure in all catalysts. Pattern (d) assignable to S4 shows more obvious diffraction peaks of Pt than these of S3, which illustrates that Pt nanoparticles have higher crystallinity after the CRP. Moreover, the peaks of TiC are also clearly observed in all catalysts and the peaks of anatase are observed in S2, S3, and S4 catalysts. The presence of sharp peak at 26.1° in the XRD patterns of S3 and S4 corresponds to CNTs (0 0 2), which is in accordance with the results in our previous work [32]. The intensity of diffraction peaks at the Bragg angles of about 25° ascribed to amorphous carbon in pattern (d) is stronger than that of pattern (c), indicating that the carbon layers are formed during the CRP.

Obvious peaks of Pt element can be clearly seen in all EDAX patterns presented in Fig. 2, indicating Pt nanoparticles were deposited onto all the supports in our experimental conditions. The Pt contents are 20.4 wt.%, 20.2 wt.%, 20.3 wt.%, and 20.0 wt.% in S1, S2, S3, and S4 catalysts, respectively, which are similar to the theoretical values. Moreover, O elements were distinctly detected in S2, S3, and S4 catalysts, illustrating that TiO_2 existed in all of S2, S3 and S4 catalysts.

Fig. 3 presents the TEM images with associated size distributions of S1, S3, and S4 catalysts before and after APCT, respectively. It can be clearly seen from Fig. 3(a) that the distribution of Pt nanoparticles of S1 is very uniform, further indicating that Pt nanoparticles can be well deposited onto the TiC surface. Moreover, it can be also evidently seen from Fig. 3(c) that the distribution of Pt nanoparticles of S3 is more uniform than that of Pt/MWCNTs [32], which is attributed to the fact that TiO_2 inside MWCNTs modifies the surface of MWCNTs and then augments the deposition sites of Pt nanoparticles [32]. The mean size of Pt nanoparticles of S3 is 0.46 nm smaller than that of Pt/MWCNTs [32]. In addition, after the CRP, the crystallite size of S4 increases by only 0.61 nm, showing that CRP effectively anchors the crystallites and inhibits migration and coalescence of the Pt nanoparticles [30–32]. As for the TEM pictures after 1000 cycles APCT, it can be obviously seen that the crystallite sizes of S1, S3, and S4 grow to 4.34 nm, 4.76 nm, and 4.54 nm, increasing by 56.7%, 28.0%, and 4.8% in comparison with those before APCT, respectively. Furthermore, after 7500 cycles APCT, the particle size of S4 increases to 6.61 nm, increasing by 52.6% compared with that before APCT. The results of TEM are consistent with the results of electrochemical measurements discussed below. According to the experimental results, the stability of S3 is higher than S1, which is ascribed to three major factors: (1) the excellent mechanical resistance and stability of TiO_2 and MWCNTs in acidic and oxidative environments; (2) the formation of criss-crossed reticular structure by TiC and nanocapsule composite MWCNTs@TiO_2 can rapidly transfer the electrons and then reduce ohmic polarization; (3) Strong metal–support interaction [33–36] between Pt nanoparticles and nanocapsule composite MWCNTs@TiO_2. Apart from these factors mentioned above, there is one more critical reason that the riveted carbon formed during the CRP effectively anchors the crystallites and inhibits migration and coalescence of the Pt nanoparticles during the APCT [30,31,32] for the ultrahigh stability of S4.

Fig. 4 shows the deconvoluted Pt 4f, C 1s, O 1s, and Ti 2p peaks from XPS analysis of S3 and S4 catalysts, respectively. The

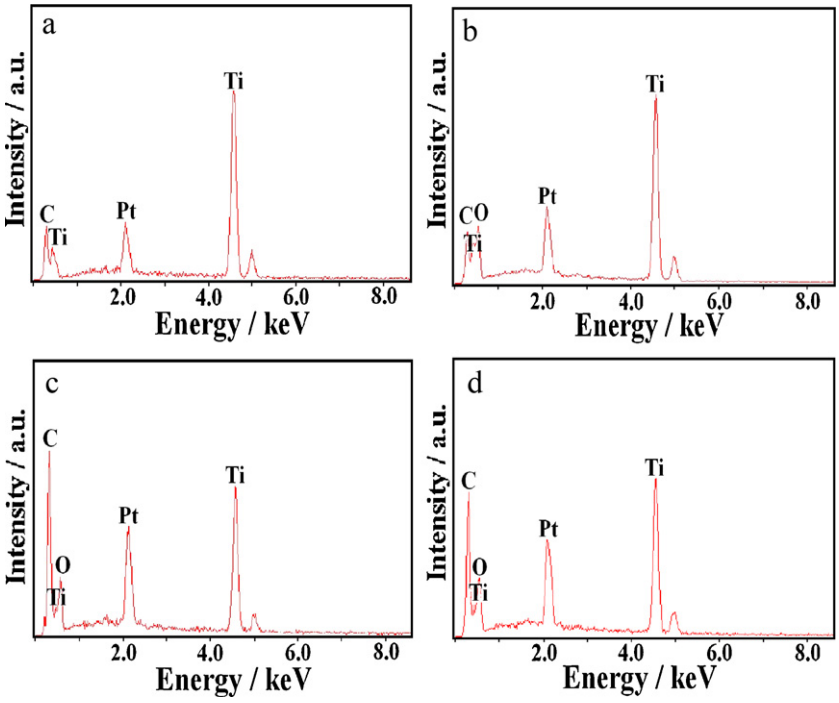

Fig. 2. EDAX patterns of S1 (a), S2 (b), S3 (c), and S4 (d) catalysts.

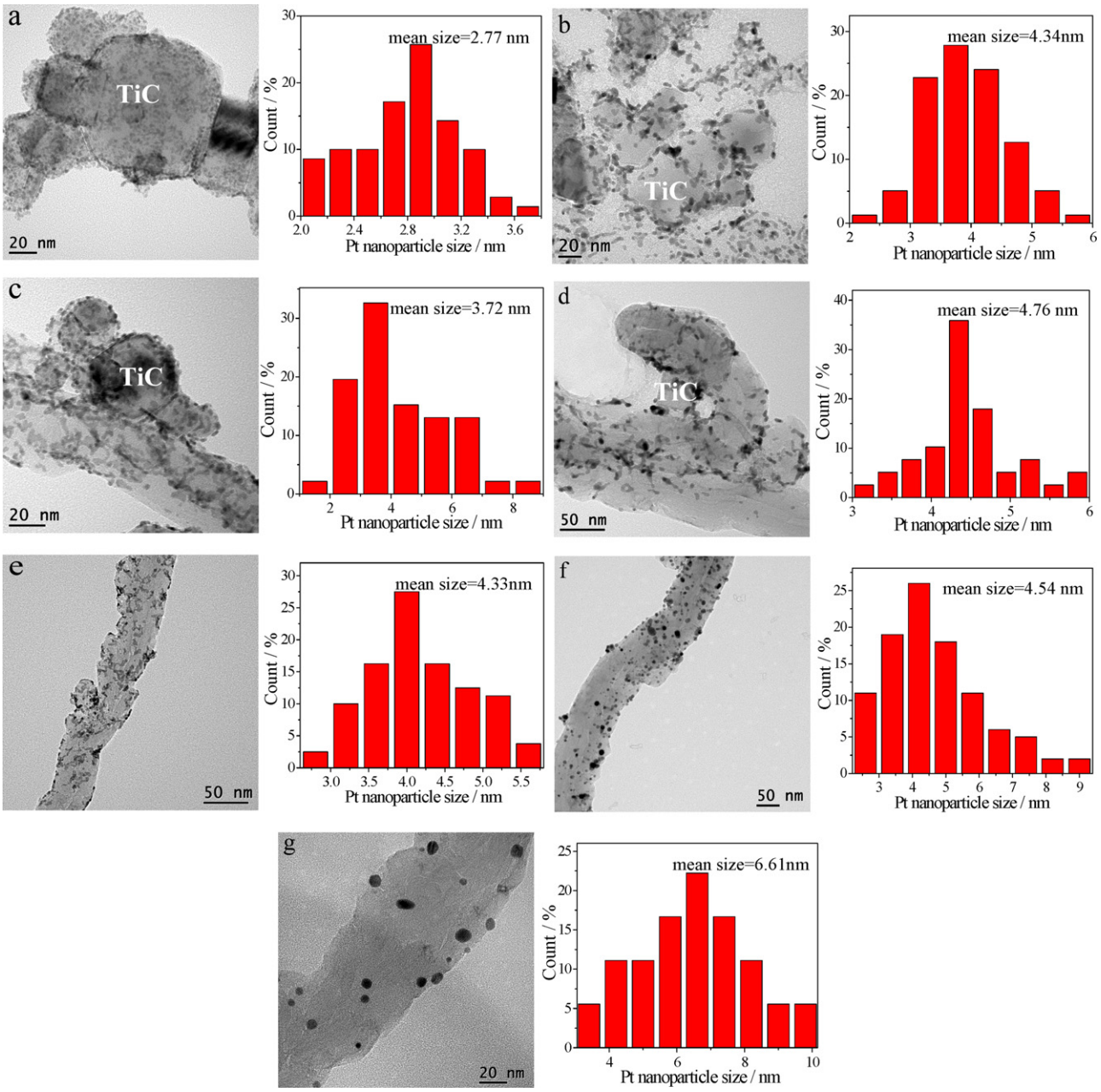

Fig. 3. TEM images and the size distributions of S1 (a, b), S3 (c, d) and S4 (e, f, g) before (a, c, e) and after (b, d, f, g) APCT, (b, d, f) after 1000 cycles APCT, (g) after 7500 cycles APCT.

curves fitting of Pt 4f, and O 1s peaks of the X-ray photoelectron spectra for S3 and S4 catalysts are in agreement with our previous reports [30–32]. However, in the curve fitting results of C 1s peaks of the X-ray photoelectron spectra, the Gaussian peak centered at 282.00 eV corresponds to TiC [36,37], which is different from our earlier results [30–32]. The binding energies of each component along with their relative intensities are provided in Tables 1–3, and Table 4, respectively. In Table 1, the Pt (0) peaks of S3 and S4 catalysts show a shift of the Pt 4f binding energy to the direction of higher energies by about 0.24 eV in comparison with that of Pt/TiC (see supporting information for details) because there is strong metal–support interaction between Pt nanoparticles and TiO_2 [33–36]. Moreover, the content of Pt (0) increases by 10.35% accompanied with decreasing by 2.49% of Pt (IV), demonstrating

Table 1
Results of the fits of the Pt 4f spectra, values given in % of total intensity.

Sample	Pt (0) 71.5 eV	Pt (II) 72.5 eV	Pt (IV) 74.3 eV
S3	63.82	22.03	14.14
S4	74.17	14.18	11.65

Table 2
Results of the fits of the C 1s spectra, values given in % of total intensity.

Sample	TiC 282.0 eV	sp^2-C 284.5 eV	sp^3-C 285.2 eV	C—OR 286.1 eV
S3	1.83	62.56	13.44	11.65
S4	2.26	57.23	24.21	12.72

Sample	C=O 287.6 eV	COOR 288.8 eV	Anti π bond 291.0 eV
S3	4.62	3.95	1.95
S4	0.21	2.26	1.11

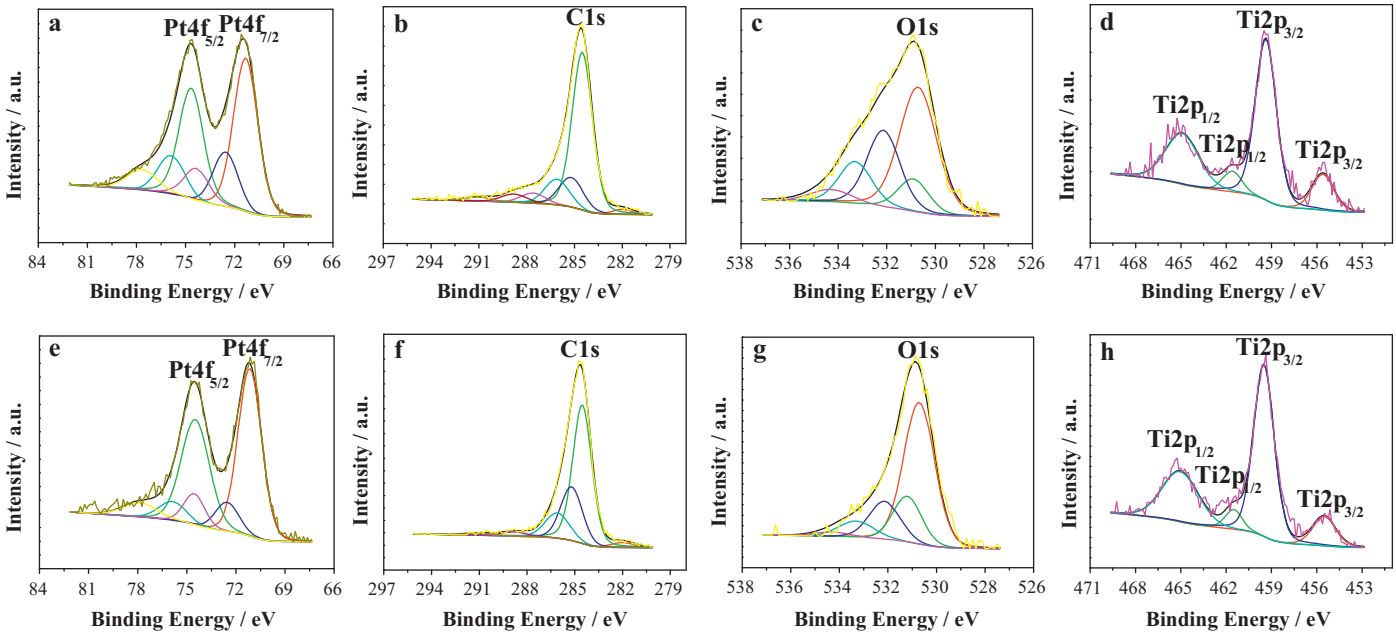

Fig. 4. Deconvoluted Pt 4f (a, e), C 1s (b, f), O1s (c, g), and Ti 2p (d, h) peaks from XPS analysis of S3 (a, b, c, d) and S4 (e, f, g, h) catalysts.

Table 3
Results of the fits of the O 1s spectra, values given in % of total intensity.

Sample	530.4 eV	531.0 eV	532.4 eV
S3	51.75	8.63	17.25
S4	52.38	13.61	21.77

Sample	533.3 eV	534.3 eV
S3	15.90	6.47
S4	9.52	2.72

Table 4
Results of the fits of the Ti 2p spectra, values given in % of total intensity.

Sample	455.6 eV	459.4 eV	461.6 eV	464.9 eV
S3	11.93	54.79	5.89	27.39
S4	10.04	56.66	4.99	28.30

that S4 catalyst has higher stability relative to S3 ascribed to more corrosion-resistant Pt (0) [17]. In addition, the curve fitting of Ti 2p peaks of the Ti X-ray photoelectron spectra before and after the CRP can be deconvoluted into four Gaussian centered at 455.60 eV, 461.60 eV, 459.37 eV, and 464.91 eV, which correspond to TiC and TiO_2 [36–38], respectively. The XPS results of C1s spectra show that the relative intensities of oxygen containing functional groups of S4 catalyst are 5.03% lower than those of S3, indicating that the carbonization of the glucose is thorough in the CRP. Furthermore, it is also clearly seen in Table 2 that sp^3-C in S4 catalyst is 10.77% greater than that in S3 catalyst. This may be one of the critical reasons for the ultrahigh stability of S4 catalyst [31,32].

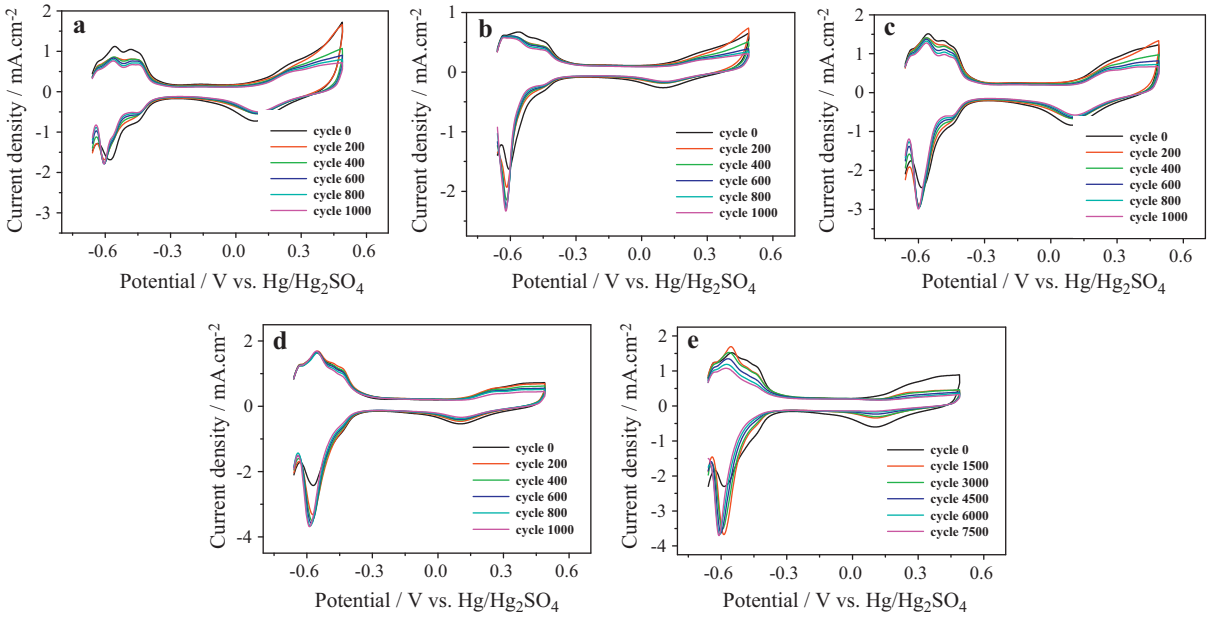

Fig. 5. CV in 0.5 mol L^{-1} H_2SO_4 for S1 (a), S2 (b), S3 (c) and S4 (d, e) catalysts during the APCT. Scanning rate: 50 mV s^{-1}; Test temperature: 25 °C.

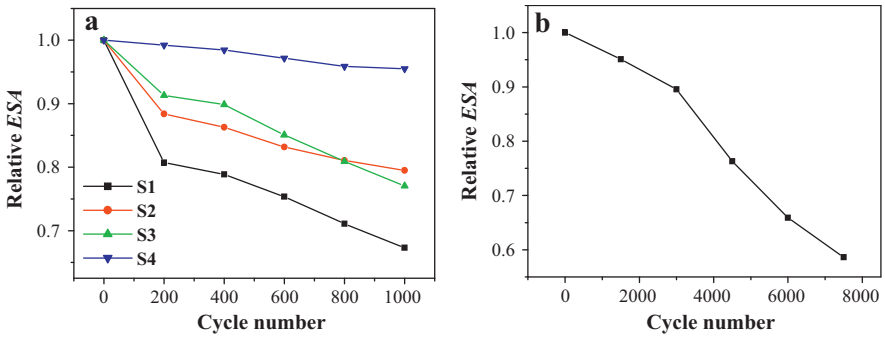

Fig. 6. Relationship of ESA and cycle number for S1 (a), S2 (a), S3 (a) and S4 (a, b) catalysts during the APCT.

Supplementary material related to this article found, in the online version, at http://dx.doi.org/10.1016/j.apcatb.2012.04.040.

In our previous study [32], the nanocapsule support of MWCNTs@TiO_2 has been confirmed through several kinds of physical characterizations including XRD, EDAX, TEM, XPS, thermal gravimetric analysis/differential thermal analysis (TGA/DTA), high angle annular dark field scanning transmission electron microscopy (HAADF-STEM) and high-resolution transmission electron microscopy (HR-TEM). Here, TiO_2 was also not detected from the surface of MWCNTs in TEM figures and there was no TiO_2 independent of MWCNTs in all carbon film field during the TEM test period. However, TiO_2 was detected obviously in XRD, EDAX, and XPS patterns, respectively, illustrating that TiO_2 should enter the inside of MWCNTs and forms the nanocapsule composite of MWCNTs with TiO_2. However, TiC can be clearly seen in TEM pictures because of its larger particle size. Consequently, as shown in Fig. 3, during the synthetic process the mixed support of TiC and nanocapsule MWCNTs@TiO_2 was formed and the S3 catalyst was synthesized.

Cyclic voltammograms for S1, S2, S3, and S4 catalysts before and after APCT are carried out in 0.5 mol L^{-1} H_2SO_4 at 25 °C and shown in Fig. 5. Measurements of the hydrogen adsorption–desorption (HAD) integrals are used to provide the electrochemically active specific surface areas of Pt nanoparticles. The variations of the ESA values calculated from the hydrogen desorption integrals with cycle number during the APCT are presented in Figs. 6 and 7. Though standard HAD regions of Pt are presented on S1 catalyst, the ESA of S1 is 60.97 m^2 $g_{Pt}{}^{-1}$ before APCT from Fig. 5(a) due to the ecumenical conductivity of TiC. The ESA of S2 is only 37.28 m^2 $g_{Pt}{}^{-1}$ before APCT from Fig. 5(b) ascribed to poor conductivity of TiO_2 in the mixed support. The ESA of S3 before APCT reaches as high as 83.56 m^2 $g_{Pt}{}^{-1}$ that is higher than 81.54 m^2 $g_{Pt}{}^{-1}$ of Pt/C [31] and 78.29 m^2 $g_{Pt}{}^{-1}$ of Pt/MWCNTs [32] by the same procedure, which is attributed to more uniform dispersion of Pt nanoparticles on the mixed support by the MAPP. Pt nanoparticles are more easily to be deposited on TiO_2 surface than on MWCNTs and TiC because of the stronger hydrophilicity of TiO_2. Then if there was TiO_2 independent of MWCNTs and TiC, the activity of S3 catalyst would be lower than Pt/MWCNTs [32] due to less Pt nanoparticles on the MWCNTs and TiC. And the high activity of S3 catalyst indicates further that there was no TiO_2 independent of MWCNTs, confirming further that TiO_2 entered into the inside of MWCNTs. Refered to S4 catalyst, its ESA before APCT is 81.52 m^2 $g_{Pt}{}^{-1}$, which is very close to that of S3, demonstrating that the mean size of Pt nanoparticles does not increase evidently in the CRP, which is in agreement with those results of TEM above. From Fig. 6, it can be clearly seen that ESA of S1 decreases by 32.7% after 1000 cycles APCT because there is no SMSI between Pt and TiC. However, ESA of S2 reduces 20.5% after 1000 cycles APCT ascribed to the SMSI between Pt and TiO_2 [33–36]. Moreover, it can be clearly seen that ESA of S3 reduces 23.0% after 1000 cycles APCT. However, ESA of S4 decreases by only 4.5% after the same tests, showing that S4 catalyst has much higher stability than S3 with similar activity. Furthermore, ESA of S4 catalyst reduces 23.7% after 4500 cycles APCT and decreases by 41.4% after 7500 cycles APCT. According to our previous report [31], ESA of Pt/C and carbon riveted Pt/TiO_2–C decreases by 49.2% and 22.3% after 1000 cycles APCT, respectively. The ESA of carbon riveted nanocapsule Pt/MWCNTs@TiO_2 catalyst reduces 21.4% after 3000 cycles APCT and decreases by 47.1% after 7500 cycles APCT, respectively [32], showing that the carbon riveted nanocapsule Pt/MWCNTs@TiO_2 catalyst possesses 7.5 times stability as high as that of Pt/C [30] and has 3 times life-span as long as that of carbon riveted Pt/TiO_2–C [31]. However, in terms of the results of electrochemical and physical characterizations, S4 catalyst exhibits 8.5 times stability as high as that of Pt/C [31] and has 4.5 times life-span as long as that of carbon riveted Pt/TiO_2–C [31]. The results may prolong the lifetime of PEMFCs and accelerate the commercialization of PEMFC to some extend.

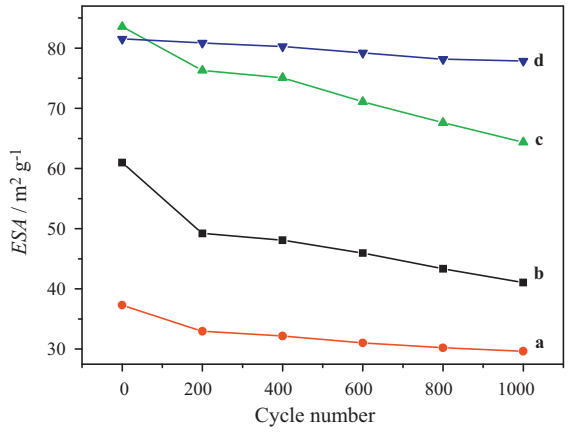

Fig. 7. ESA as a function of cycle number for S2 (a), S1 (b), S3 (c) and S4 (d) catalysts during the APCT.

4. Conclusions

Pt/TiC, Pt/TiO_2–TiC, Pt/MWCNTs@TiO_2–TiC catalysts have been synthesized by the microwave-assisted polyol process. Both of the activity and stability of Pt/TiC cannot meet the requirements of proton exchange membrane fuel cells. In comparison with Pt/TiC, Pt/TiO_2–TiC catalyst exhibits lower activity due to poor conductivity of TiO_2 and higher stability ascribed to strong metal–support interaction between Pt and TiO_2. In addition, compared with Pt/TiC, Pt/MWCNTs@TiO_2–TiC catalyst exhibits both higher activity and stability because of high electrical conductivity of the mixed support and the SMSI between Pt and nanocapsule

support MWCNTs@TiO_2. The carbon riveted Pt/MWCNTs@TiO_2–TiC exhibits 8.5 times stability as high as that of Pt/C and has 4.5 times life-span as long as that of carbon riveted Pt/TiO_2–C reported in our previous work. The significantly enhanced stability for carbon riveted Pt/MWCNTs@TiO_2–TiC catalyst is attributed to five critical reasons: (1) the inherently excellent mechanical resistance and stability of TiC, TiO_2, and MWCNTs in acidic and oxidative environments; (2) the formation of criss-crossed reticular structure by TiC and nanocapsule composite MWCNTs@TiO_2 can rapidly transfer the electrons and then reduce ohmic polarization; (3) SMSI between Pt nanoparticles and nanocapsule composite; (4) the anchoring effect of carbon layers formed during the carbon riveting process; (5) the increase of Pt (0) composition during the CRP. Considering both of the high activity and stability of carbon riveted Pt/MWCNTs@TiO_2–TiC catalyst, this kind of catalyst will be a promising catalyst for PEMFCs.

Acknowledgments

This project is financially supported by the National Natural Science Foundation of China (Grant No. 20606007), the Scientific Research Foundation for the Returned Overseas Chinese Scholars, State Education Ministry (2008), and Scientific Research Foundation for Returned Scholars of Heilongjiang Province of China (Grant No. LC08C33).

References

[1] P. Hernández-Fernández, M. Montiel, P. Ocón, J.L.G. de la Fuente, S. García-Rodríguez, S. Rojas, J.L.G. Fierro, Applied Catalysis B: Environmental 99 (2010) 343–352.
[2] S.-Y. Huang, P. Ganesan, B.N. Popov, Applied Catalysis B: Environmental 102 (2011) 71–77.
[3] J. Lobato, P. Cañizares, D. Ubeda, F.J. Pinar, M.A. Rodrigo, Applied Catalysis B: Environmental 106 (2011) 174–180.
[4] D.H. Lim, W.D. Lee, D.H. Choi, H.I. Lee, Applied Catalysis B: Environmental 94 (2010) 85–96.
[5] G. Liu, X.G. Li, P. Ganesan, B.N. Popov, Applied Catalysis B: Environmental 93 (2009) 156–165.
[6] A. Morozan, B. Jousselme, S. Palacin, Energy & Environmental Science 4 (2011) 1238–1254.
[7] J. Zhao, A. Manthiram, Applied Catalysis B: Environmental 101 (2011) 660–668.
[8] Y.Y. Shao, G.P. Yin, Y.Z. Gao, Journal of Power Sources 171 (2007) 558–566.
[9] S.S. Zhang, X.Z. Yuan, J.N.C. Hin, H.J. Wang, K.A. Friedrich, M. Schulze, Journal of Power Sources 194 (2009) 588–600.
[10] S. Yin, S. Mu, H. Lv, N. Cheng, M. Pan, Z. Fu, Applied Catalysis B: Environmental 93 (2010) 233–240.
[11] R. Borup, J. Meyers, B. Pivovar, Y.S. Kim, R. Mukundan, N. Garland, D. Myers, M. Wilson, F. Garzon, D. Wood, P. Zelenay, K. More, K. Stroh, T. Zawodzinski, J. Boncella, J.E. McGrath, M. Inaba, K. Miyatake, M. Hori, K. Ota, Z. Ogumi, S. Miyata, A. Nishikata, Z. Siroma, Y. Uchimoto, K. Yasuda, K.I. Kimijima, N. Iwashita, Chemical Reviews 107 (2007) 3904–3951.
[12] S.H. Joo, S.J. Choi, I. Oh, J. Kwak, Z. Liu, O. Terasaki, R. Ryoo, Nature 412 (2001) 169–172.
[13] M.S. Saha, R. Li, X. Sun, Journal of Power Sources 177 (2008) 314–322.
[14] Y. Shao, J. Liu, Y. Wang, Y. Lin, Journal of Materials Chemistry 19 (2009) 46–59.
[15] Z.B. Wang, G.P. Yin, P.F. Shi, Carbon 44 (2006) 133–140.
[16] Z.-Z. Jiang, D.-M. Gu, Z.-B. Wang, W.-L. Qu, G.-P. Yin, K.-J. Qian, Journal of Power Sources 196 (2011) 8207–8215.
[17] W. Li, A.M. Lane, Electrochemistry Communications 11 (2009) 1187–1190.
[18] S. Maass, F. Finsterwalder, G. Frank, R. Hartmann, C. Merten, Journal of Power Sources 176 (2008) 444–451.
[19] L.M. Roen, C.H. Paik, T.D. Jarvi, Electrochemical and Solid-State Letters 7 (2004) A19–A22.
[20] J. Chen, K. Takanabe, R. Ohnishi, D. Lu, S. Okada, H. Hatasawa, H. Morioka, M. Antonietti, J. Kubota, K. Domen, Chemical Communications 46 (2010) 7492–7494.
[21] X. Cui, J. Shi, H. Chen, L. Zhang, L. Guo, J. Gao, J. Li, Journal of Physical Chemistry B 112 (2008) 12024–12031.
[22] K.-F. Zhang, D.-J. Guo, X. Liu, J. Li, H.-L. Li, Z.-X. Su, Journal of Power Sources 162 (2006) 1077–1081.
[23] H. Chhina, S. Campbell, O. Kesler, Journal of Power Sources 161 (2006) 893–900.
[24] C. Liang, L. Ding, C. Li, M. Pang, D. Su, W. Li, Y. Wang, Energy & Environmental Science 3 (2010) 1121–1127.
[25] M.C. Orilall, F. Matsumoto, Q. Zhou, H. Sai, H.D. Abruña, F.J. DiSalvo, U. Wiesner, Journal of the American Ceramic Society 131 (2009) 9389–9395.
[26] S. Yang, N. Chen, W. Liu, M. Zhong, Z. Wang, H. Kokawa, Surface and Coatings Technology 183 (2004) 254–260.
[27] X.H. Wang, M. Zhang, X.M. Liu, S.Y. Qu, Z.D. Zou, Surface and Coatings Technology 202 (2008) 3600–3606.
[28] L. Ma, S. Sui, Y. Zhai, Journal of Power Sources 177 (2008) 470–477.
[29] Y.-Y. Chu, Z.-B. Wang, D.-M. Gu, G.-P. Yin, Journal of Power Sources 195 (2010) 1799–1804.
[30] Z.-Z. Jiang, Z.-B. Wang, D.-M. Gu, E.S. Smotkin, Chemical Communications 46 (2010) 6998–7000.
[31] Z.-Z. Jiang, Z.-B. Wang, Y.-Y. Chu, D.-M. Gu, G.-P. Yin, Energy & Environmental Science 4 (2011) 728–735.
[32] Z.-Z. Jiang, Z.-B. Wang, Y.-Y. Chu, D.-M. Gu, G.-P. Yin, Energy & Environmental Science 4 (2011) 2558–2566.
[33] S.J. Tauster, S.C. Fung, R.T.K. Baker, J.A. Horsley, Science 211 (1981) 1121–1125.
[34] J.-M. Herrmann, P. Pichat, Journal of Catalysis 78 (1982) 425–435.
[35] A. Dauscher, L. Hilaire, F. Le Normand, W. Müller, G. Maire, A. Vasquez, Surface and Interface Analysis 16 (1990) 341–346.
[36] A.A. El Mel, B. Angleraud, E. Gautron, A. Granier, P.Y. Tessier, Surface and Coatings Technology 204 (2010) 1880–1883.
[37] A.A. El Mel, B. Angleraud, E. Gautron, A. Granier, P.Y. Tessier, Thin Solid Films 519 (2011) 3982–3985.
[38] D.A. Peña, B.S. Uphade, P.G. Smirniotis, Journal of Catalysis 221 (2004) 421–431.